



RESEARCH

# A contact force calculation approach for collision analysis with zero or non-zero initial relative velocity

Yinhua Shen · Dong Xiang

Received: 5 April 2024 / Accepted: 22 July 2024 / Published online: 1 August 2024  
© The Author(s), under exclusive licence to Springer Nature B.V. 2024

**Abstract** The computation of contact force between elastic bodies is the key to analyzing non-stationary vibrations in mechanical system and warrants further research. To establish a contact force calculation approach suitable for elastic bodies under external forces, the contact state is categorized into three types by analyzing energy conversion during the elastic contact process: collision contact without external forces, collision contact with zero initial relative velocity, and collision contact considering external forces. For the first type, a hysteresis damping factor is derived based on energy restitution coefficients and numerical analysis, which maintains high accuracy even with low restitution coefficients. Next, an iterative calculation approach combining the bisection and Newton's methods is developed for the second type. On this basis, a numerical computation process is subsequently proposed for the third type. To demonstrate the utility of the proposed approach, dynamic characteristics analysis of simultaneous collisions and multiple continuous collisions are presented as case studies. The results confirm the effectiveness of this calculation approach.

**Keywords** Collision contact · Contact force calculation · Bisection method · Newton's method · Simultaneous collisions

## 1 Introduction

In stable mechanical systems, elastic bodies subject to external disturbances often exhibit vibrations or oscillations. These interactions can exacerbate into more severe collision phenomena due to clearances between the bodies. Factors such as damping can dissipate the energy from these collisions and vibrations, restoring the system to a stable state. However, collisions and oscillations significantly affect the contact state between elastic bodies, potentially leading to noise, fatigue, and wear, thereby endangering the system's stability. Consequently, extensive research [1–6] has been dedicated to addressing contact issues under such unstable conditions.

As a common contact type in mechanical systems, collision involves two elastic bodies meeting at a specific initial relative velocity to undergo compression and restitution deformation. The force generated during collision contact is vital for analyzing the dynamic response of collisions, prompting the development of numerous models for simulating collision dynamics. Among them, models based on spring-damping element are widely used. A simple one is the Kelvin-Voigt model which was employed by Khulief

---

Y. Shen (✉)  
Army Logistics Academy, Chongqing 401331, China  
e-mail: cheninh14@tsinghua.org.cn

D. Xiang  
The School of Mechanical Engineering, University of  
Science and Technology Beijing, Beijing 100083, China

and Shabana [7] for impact analysis in multibody system. However, this linear model has short in representing the overall nonlinear nature of contact. In contrast, Hunt and Crossley [8] established a nonlinear contact force model combining Hertzian contact force and damping force. This had spurred a series of improved models tailored by researchers for specific purposes, like the Lee and Wang model [9], the Lankarani and Nikravesh model [10], and other models [11–16] up to the Zhang et al. model [17]. These models primarily focus on accurately representing energy loss during collision through damping forces, typically using Newton's restitution coefficient to derive the key parameter of hysteresis damping factor. However, reference [18] argues that Newton's restitution coefficient is not suitable for collision processes under external forces, and recommending the use of the energy restitution coefficient [19] to model forces in such scenarios. Moreover, this reference also believes that external forces and collision energy loss are the key factors that cause collision state to end, and applies the established quantitative judgment to identify two collision end states—separation and non-separation.

When non-separation occurs, the elastic bodies continue their compression and restitution deformation under cyclic external forces. In other words, there exists a special collision contact state between elastic bodies when there is no initial relative velocity, termed here as NIRV-collision contact. Although some studies, like gear meshing forces [20–22], utilize the Kelvin-Voigt model for NIRV-collision scenarios, significant simulation errors are evident when collision models are improperly applied. For instance, Warzecha [23] used Michalczyk model [24] and Zhang model [17] to simulate the multi-zone collisions of a collinear system consisting of six particles, resulting in frequently changing and incomprehensible NIRV-collision contact forces. It should be noted that it is difficult to clearly express energy dissipation for NIRV-collision contact, thus, Carretero-González et al. [25] have made strides in this area by using experimental data to establish a dissipation coefficient for NIRV-collision force models in multi-particle collision systems. Therefore, the contact force model required for non-stationary dynamic analysis considering both collision and NIRV-collision needs further research.

The purpose of this article is to establish a contact force calculation approach applicable to collision and NIRV-collision dynamic analysis. It begins by elaborating the overarching issue of modeling contact

forces under external influences. Then, examines the collision process with only the initial relative velocity considered, and establishes a model for collision contact without external forces. Building on this foundation, it develops a method for calculating collision and NIRV-collision contact forces under varying external conditions and proposes a corresponding numerical process. The effectiveness of this approach is demonstrated through dynamic analysis of simultaneous and multiple continuous collisions, underscoring the model's practical relevance.

## 2 General issues of contact force model

The one-dimensional direct central frictionless contact between two elastic spheres is utilized to analyze the collision and NIRV-collision, as illustrated in Fig. 1, where the masses of the two elastic spheres are represented as  $m_i$  and  $m_j$ , respectively. When subjected to variable external forces  $F_i(t)$  and  $F_j(t)$ , the two elastic spheres start to contact at velocities  $v_i^{(-)}$  and  $v_j^{(-)}$ , respectively, then deformation takes place in the local contact area, and this denotes the start of compression phase. According to Hertz force and damping force, the contact force between these two spheres can be expressed

$$F_n = k\delta^3 + \mu\delta^3\dot{\delta} \quad (1)$$

where  $\delta$  is the local deformation,  $k$  denotes the contact stiffness,  $\dot{\delta}$  represents the deformation velocity, and  $\mu$  is the hysteresis damping factor which plays a crucial role in modeling contact force.

At this point, the external forces begin to do work, and along with the initial relative kinetic energy, are converted into elastic deformation potential energy, relative kinetic energy, and work done by the damping force, as shown

$$\frac{1}{2}m_e(\dot{\delta}^{(-)})^2 + \int_0^{\delta} F_e(t)d\delta = \frac{2}{5}k\delta^5 + \frac{1}{2}m_e\dot{\delta}^2 + \int_0^{\delta} \mu\delta^3\dot{\delta}d\delta \quad (2)$$

where  $F_e(t) = F_i(t) - F_j(t)$  is the equivalent external force,  $\int_0^{\delta} F_e(t)d\delta$  denotes the work done by equivalent external force,  $\dot{\delta}^{(-)} = v_i^{(-)} - v_j^{(-)}$  and  $m_e(\dot{\delta}^{(-)})^2/2$

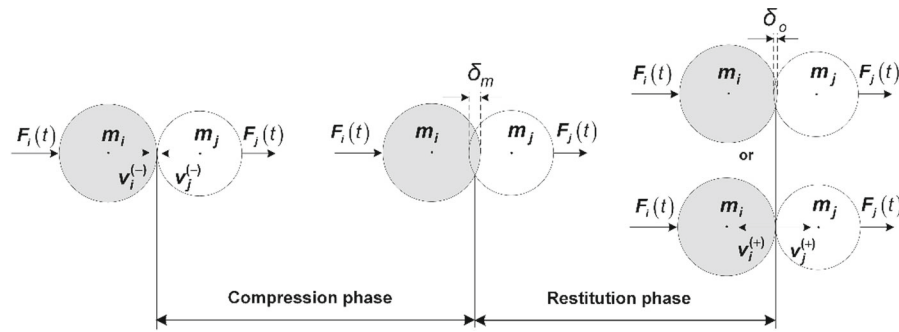


**Fig. 1** Collision process between two elastic spheres under external forces

represent the initial relative velocity and the initial relative kinetic energy, respectively, whereas  $2k\delta^{5/2}/5$ ,  $m_e\dot{\delta}^2/2$  and  $\int_0^{\delta} \mu\delta^{3/2}\dot{\delta}d\delta$  are the elastic deformation potential energy, the relative kinetic energy, and the work done by damping force, respectively.

As the deformation peaks, the deformation velocity reaches zero, and the accumulated potential and kinetic energies alongside the work done by the damping force reach their respective maxima. Thus, the energy balance at the end of the compression phase is

$$\frac{1}{2}m_e\left(\dot{\delta}^{(-)}\right)^2 + \int_0^{\delta_m} F_e(t)d\delta = \frac{2}{5}k\delta_m^{5/2} + \int_0^{\delta_m} \mu\delta^{3/2}\dot{\delta}d\delta \quad (3)$$

where  $2k\delta_m^{5/2}/5$  is the maximum elastic deformation potential energy,  $\int_0^{\delta_m} \mu\delta^{3/2}\dot{\delta}d\delta$  and  $\int_0^{\delta_m} F_e(t)d\delta$  denote the work done by damping force and the work done by equivalent external force during the compression phase, respectively.

Subsequently, the deformation begins to diminish, indicating the start of the restitution phase. The energy balances during and at the end of this phase can be respectively expressed as

$$\frac{2}{5}k\delta_m^{5/2} = \frac{2}{5}k\delta^{5/2} + \int_{\delta}^{\delta_m} \mu\delta^{3/2}|\dot{\delta}|d\delta + \int_{\delta}^{\delta_m} F_e(t)d\delta + \frac{1}{2}m_e\dot{\delta}^2 \quad (4)$$

$$\frac{2}{5}k\delta_m^{5/2} = \int_0^{\delta_m} \mu\delta^{3/2}|\dot{\delta}|d\delta + \int_0^{\delta_m} F_e(t)d\delta + \frac{1}{2}m_e\left(\dot{\delta}^{(+)}\right)^2 \quad (5)$$

where  $\dot{\delta}^{(+)}$  is the separation velocity,  $m_e\left(\dot{\delta}^{(+)}\right)^2/2$  denotes the relative separation kinetic energy, and  $\int_0^{\delta_m} \mu\delta^{3/2}|\dot{\delta}|d\delta$  represents the work done by damping force in restitution phase.

Substituting Eq. (5) into Eq. (3) yields

$$\frac{1}{2}m_e\left(\dot{\delta}^{(-)}\right)^2 + \int_0^{\delta_m} F_e(t)d\delta = \int_0^{\delta_m} F_e(t)d\delta + \frac{1}{2}m_e\left(\dot{\delta}^{(+)}\right)^2 + \int_0^{\delta_m} \mu\delta^{3/2}\dot{\delta}d\delta \quad (6)$$

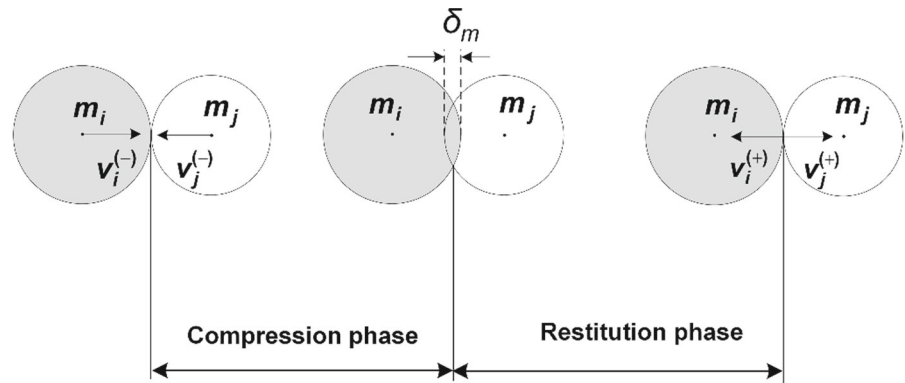
where  $\int_0^{\delta_m} \mu\delta^{3/2}\dot{\delta}d\delta$  is the work done by damping force throughout the entire contact process, which is also considered as the energy loss during a compression and restitution cycle, and how to calculate this energy loss is important to deriving contact force model.

It is crucial to acknowledge that the energy balance shown in Eq. (6) can manifest in three distinct situations: ① Ignoring the work done by the equivalent external force; ② Considering cases where the initial relative kinetic energy is zero; ③ Accounting these two energies simultaneously. In the following sections, the contact forces for these three situations will be analyzed respectively.

### 3 Collision contact hysteresis damping factor without external forces

The collision system that ignores external forces is a commonly used system for modeling collision force, as shown in Fig. 2. Based on this system, Flores et al. [26], Hu and Guo [27] constructed typical collision contact force models, with key steps including

**Fig. 2** Collision system without external forces



derivations of deformation velocity and hysteresis damping factor.

For the deformation velocity, the energy balance shown in Eqs. (2) and (3) can be rewritten as

$$\frac{1}{2}m_e(\dot{\delta}^{(-)})^2 = \frac{2}{5}k\delta^{\frac{5}{2}} + \frac{1}{2}m_e\dot{\delta}^2 + \int_0^{\delta} \mu\delta^{\frac{3}{2}}\dot{\delta}d\delta \quad (7)$$

$$\frac{1}{2}m_e(\dot{\delta}^{(-)})^2 = \frac{2}{5}k\delta_m^{\frac{5}{2}} + \int_0^{\delta_m} \mu\delta^{\frac{3}{2}}\dot{\delta}d\delta \quad (8)$$

Ignoring the work done by damping force, yields

$$\frac{1}{2}m_e(\dot{\delta}^{(-)})^2 = \frac{2}{5}k\delta^{\frac{5}{2}} + \frac{1}{2}m_e\dot{\delta}^2 \quad (9)$$

$$\frac{1}{2}m_e(\dot{\delta}^{(-)})^2 = \frac{2}{5}k\delta_m^{\frac{5}{2}} \quad (10)$$

Multiplying both sides of Eq. (9) by Eq. (10) results in

$$\dot{\delta} = \dot{\delta}^{(-)}\sqrt{1 - \left(\frac{\delta}{\delta_m}\right)^{\frac{5}{2}}} \quad (11)$$

Substituting Eq. (11) into the damping force work term of Eq. (8) to obtain

$$\Delta E_c = \int_0^{\delta_m} \mu\dot{\delta}^{(-)}\sqrt{1 - \left(\frac{\delta}{\delta_m}\right)^{\frac{5}{2}}}\delta^{\frac{3}{2}}d\delta \quad (12)$$

where  $\Delta E_c$  is the work done by damping force during compression phase.

Setting  $x = \delta/\delta_m$ , then Eq. (12) is transformed into

$$\Delta E_c = \frac{2}{5}\mu\dot{\delta}^{(-)}\delta_m^{\frac{5}{2}}\int_0^1 \sqrt{1 - x^{\frac{5}{2}}}dx^{\frac{5}{2}} \quad (13)$$

Calculating the integral term of the above equation to obtain

$$\Delta E_c = \frac{4}{15}\mu\dot{\delta}^{(-)}\delta_m^{\frac{5}{2}} \quad (14)$$

In addition, the collision restitution coefficient can be used to estimate the energy loss of collision, and the Stronge's model [19] shown in Eq. (15), which is also called energy model, is used here.

$$\varepsilon^2 = -\frac{W_r}{W_c} \quad (15)$$

where  $\varepsilon$  denotes the restitution coefficient,  $W_r$  and  $W_c$  are the work done by contact force in compression and restitution phases, respectively, given by

$$W_r = \int_{\delta_m}^0 F_n d\delta = -\frac{2}{5}k\delta_m^{\frac{5}{2}} + \int_{\delta_m}^0 \mu\delta^{\frac{3}{2}}\dot{\delta}d\delta \quad (16)$$

$$W_c = \int_0^{\delta_m} F_n d\delta = \frac{2}{5}k\delta_m^{\frac{5}{2}} + \int_0^{\delta_m} \mu\delta^{\frac{3}{2}}\dot{\delta}d\delta \quad (17)$$

Substituting Eqs. (16) and (17) into Eq. (15), yields

$$\varepsilon^2\Delta E_c + \Delta E_r = \frac{2}{5}(1 - \varepsilon^2)k\delta_m^{\frac{5}{2}} \quad (18)$$

where  $\Delta E_r$  is the work done by damping force in restitution phase. For  $\Delta E_r$ , considering the similarity in deformation velocity between the compression and restitution phases, and the Newtonian restitution coefficient, references [26, 27] assume  $\Delta E_r = \varepsilon\Delta E_c$  to derive the expression of the hysteresis damping factor  $\mu$ .

However, the disparities in deformation velocity between compression and restitution phases is increasing as the reduction of the restitution coefficient, as

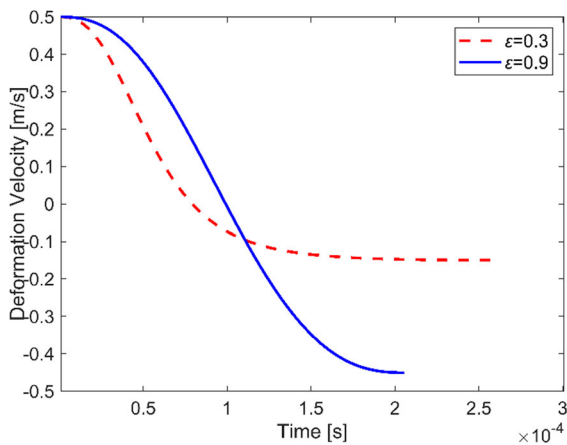


**Fig. 3** Deformation velocity

shown in Fig. 3. In turn, this difference leads to an increase in the error of the damping factor model, as shown in Fig. 4 where post- restitution coefficients are calculated by these damping factor models shown in Table 1, including Hunt and Crossley model, Lankarani and Nikravesh model, Flores et al. model, and Hu and Guo model. It should be noted that the smaller the error, the better the model accuracy.

To reduce this error, we assume that the relationship between the work done by the damping force during the restitution and compression phases is

$$\Delta E_r = \varepsilon^a \Delta E_c \tag{19}$$

where  $a$  is the constant index of restitution coefficient.

Substituting Eqs. (14) and (19) into Eq. (18) yields

$$\mu = \alpha \frac{k}{\dot{\delta}^{(-)}} \tag{20}$$

$$\alpha = \frac{3(1 - \varepsilon^2)}{2(\varepsilon^2 + \varepsilon^a)} \tag{21}$$

where  $\alpha$  is the hysteresis damping factor coefficient. It should be noted that Eq. (21) represents the Hu and Guo model when  $a$  is taken as 1, which means that the hysteresis damping factor  $\mu$  is too high when the restitution coefficient is small. Since  $\varepsilon$  generally ranges between 0 and 1,  $a$  should be adjusted below 1 to reduce the hysteresis damping factor  $\mu$ .

For a more precise  $\mu$  estimation, Eq. (22) is utilized to perform iterative calculation with  $a$  step size decrement of 0.01.

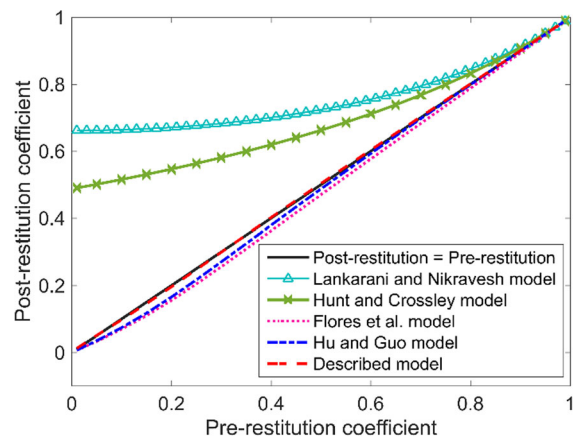


**Fig. 4** Post-restitution versus pre-restitution coefficients

**Table 1** Hysteresis damping factor model

Model	Factor $\alpha$
Hunt and Crossley [8]	$\frac{3(1-\varepsilon)}{2}$
Lankarani and Nikravesh [10]	$\frac{3(1-\varepsilon^2)}{4}$
Flores et al. [26]	$\frac{8(1-\varepsilon)}{5\varepsilon}$
Hu and Guo [27]	$\frac{3(1-\varepsilon)}{2\varepsilon}$

$$m_e \ddot{\delta} + \frac{3(1 - \varepsilon^2)}{2(\varepsilon^2 + \varepsilon^a)} \frac{k}{\dot{\delta}^{(-)}} \delta^{\frac{3}{2}} \dot{\delta} + k \delta^{\frac{3}{2}} = 0 \tag{22}$$

here,  $m_e$  is equal to 0.5 kg and  $\dot{\delta}^{(-)}$  is 0.5 m/s, whereas the value of  $k$  is  $2.41 \times 10^{10} \text{N/m}^{3/2}$ , and the restitution coefficient  $\varepsilon$  is calculated by Eq. (15). The result shows that the post-restitution coefficient is nearly identical to the pre-restitution coefficient at  $a = 0.87$ , as indicated by the dashed line in Fig. 4 where the discrepancy in the post-restitution coefficient is within 2.9% and 1.1% when the pre-restitution coefficient ranges from 0.05 to 0.3, with others error being less than 0.8%. Equation (23) presents the corresponding hysteresis damping factor, and Fig. 5 illustrates the comparative curves of the hysteresis damping factor between the Hu and Guo model and the model discussed herein.

$$\mu = \frac{3(1 - \varepsilon^2)}{2(\varepsilon^2 + \varepsilon^{0.87})} \frac{k}{\dot{\delta}^{(-)}} \tag{23}$$

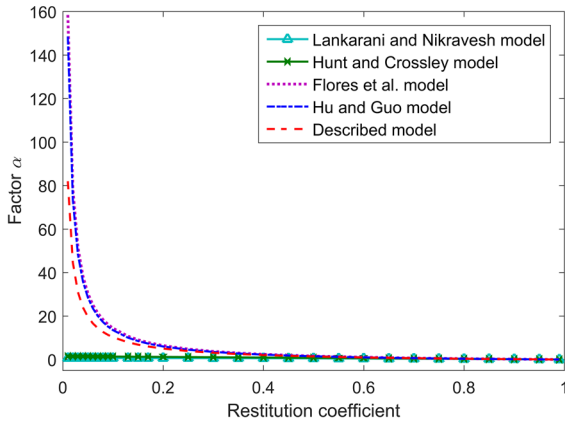


**Fig. 5** Factor  $\alpha$  versus restitution coefficient

### 4 Collision contact hysteresis damping factor considering only external forces

The collision contact considering only external forces is a special collision contact, which is described by Fig. 6. Compared to Fig. 1, the two elastic spheres start to contact with no initial relative velocity. It should be noted that there may be initial compression  $\delta_s$  between the two elastic spheres. In addition, the spheres might not fully separate at the end of a contact cycle, resulting in an inseparable state, as shown Fig. 6 where  $\delta_o$  denotes incomplete separation compression.

Combined Eqs. (16) to (17), and Eq. (6) that ignoring the initial relative velocity, yields

$$\Delta E = (1 - \varepsilon^2) \int_0^{\delta_m} F_e(t) d\delta \tag{24}$$

where  $\Delta E$  denotes the energy loss of the NIRV-collision contact.

It can be drawn from above equation that this energy loss is hard to calculate due to the influence of variable external forces. Additionally, the relationship between

$\Delta E_r$  and  $\Delta E_c$  described in Eq. (19) is difficult to derive, as is deducing the deformation velocity model. To address these complexities, we propose a calculation approach using bisection method to iteratively determine the hysteresis damping factor. The main mentality is to apply the energy restitution coefficient shown in Eq. (15) to construct a function  $f(\mu)$  with hysteresis damping factor as a variable, as shown in Eq. (25). Next, determine the value range for the function variable  $\mu$  through Eq. (26), which is  $[a, b]$ . It should be noted that  $W_{cn}$  and  $W_m$  in the function are obtained from simulations of the contact process with Eqs. (17) and (16). Then, calculate the next iteration value of  $\mu$  according to Eq. (27).

$$f(\mu_n) = \frac{W_m}{W_{cn}} + \varepsilon^2 \tag{25}$$

$$\begin{cases} a = \mu_n & f(\mu_n) < 0 \\ b = \mu_n & f(\mu_n) > 0 \end{cases} \tag{26}$$

$$\mu_{n+1} = \frac{a + b}{2} \tag{27}$$

The primary challenges in this iterative process includes setting the initial value of  $\mu$  and the iteration value before  $[a, b]$  is determined. The initial  $\mu$  value could either be  $\mu_{n-1}$  from the previous collision or  $\mu_0$  calculated from Eq. (28).

$$\mu_0 = \frac{3}{2} \frac{(1 - \varepsilon^2)}{(\varepsilon^2 + \varepsilon^{0.87})} k \tag{28}$$

For the second challenge, Eq. (29) can be employed for the iteration value, which is obtained according to the Newton method. However, this method is sensitive to the selection of initial value and there is a possibility of too many iterations. In this case, other methods can be used, such as the approach shown in Eq. (31).

**Fig. 6** Elastic contact process under external force

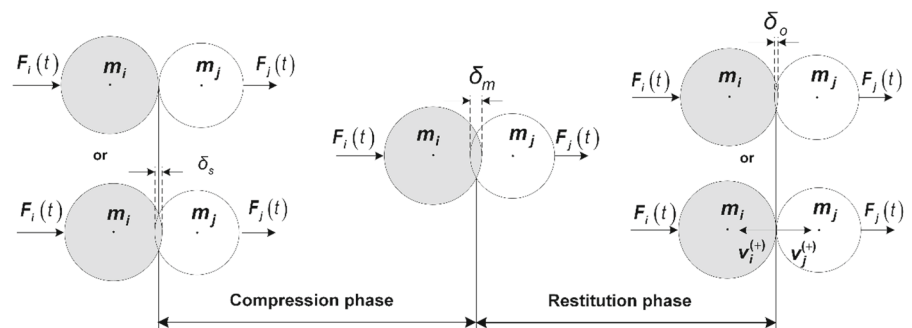
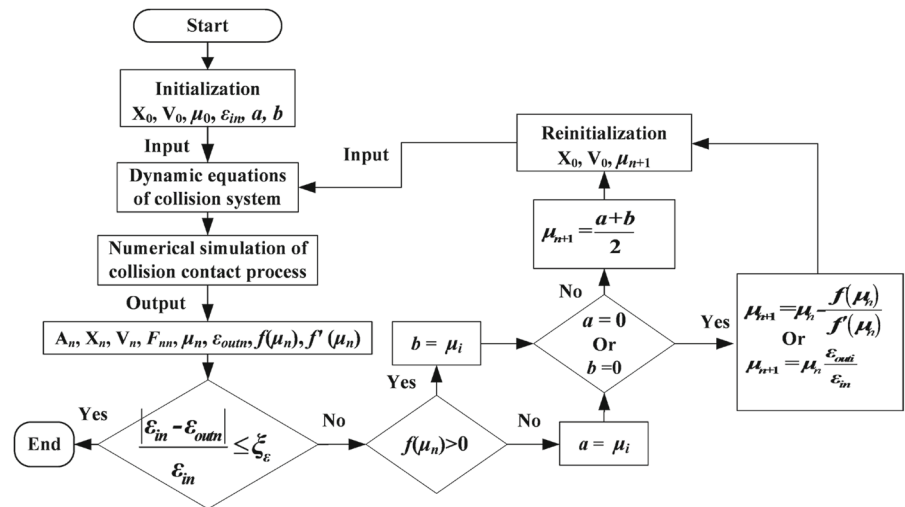


**Fig. 7** Numerical calculation process



$$\mu_{n+1} = \mu_n - \frac{f(\mu_n)}{f'(\mu_n)} \tag{29}$$

where

$$\begin{cases} f'(\mu_n) = \frac{W_{cn}S_{rn} - W_{rn}S_{cn}}{W_{cn}^2} \\ S_{cn} = \int_{\delta_s}^{\delta_m} \delta^{\frac{3}{2}} \dot{\delta} d\delta \\ S_{rn} = \int_{\delta_m}^{\delta_o} \delta^{\frac{3}{2}} \dot{\delta} d\delta \end{cases} \tag{30}$$

Equation (31) mainly considers that if the post-restitution coefficient  $\epsilon_{out}$  calculated by Eq. (15) is too larger, it indicates that  $\mu_n$  is too small, conversely,  $\mu_n$  tends to larger. Therefore, when  $\epsilon_{out}$  is greater than pre- restitution coefficient  $\epsilon_{in}$ , then  $\epsilon_{out}/\epsilon_{in}$  is greater than 1. Multiplying it by  $\mu_n$  to obtain the increased iteration value of  $\mu_{n+1}$ , and on the contrary, decreased  $\mu_{n+1}$  can be obtained.

$$\mu_{n+1} = \mu_n \frac{\epsilon_{out}}{\epsilon_{in}} \tag{31}$$

It's crucial to highlight that at the end of NIRV-collision contact, two potential states emerge: separation and non-separation. The criteria for these states during the restitution phase are discussed in reference [18], where it is noted that during the restitution phase, separation occurs when  $\delta = 0$  and  $\dot{\delta}^{(+)} \geq 0$ , and non-separation occurs when  $\delta > 0$  and  $\dot{\delta}^{(+)} = 0$ .

### 5 Calculation process for collision contact forces under external forces

In the contact system shown in Fig. 1, collisions undergo several transitions between their initiation and cessation. Due to energy loss and external forces, the strength of collision contact may gradually decrease until NIRV-collision contact occurs, and the influence of external forces on the contact process increases accordingly. This means that it is necessary to separately calculate collision contact force and NIRV-collision contact force when analyzing the dynamics of the contact system, and both need to consider the influence of external forces.

The energy loss of a collision influenced by external forces, as derived from Eqs. (6), (15) and (17), indicates multiple contributing factors, complicating the prediction of collision energy loss.

$$\Delta E = (1 - \epsilon^2) \left[ \frac{1}{2} m_e (\dot{\delta}^{(-)})^2 + \int_0^{\delta_m} F_e(t) d\delta \right] \tag{32}$$

Therefore, similar to NIRV-collision contact, the hysteresis damping factor of this contact is calculated by Eqs. (25) to (31), then substituting into Eq. (1) to determine the corresponding contact forces. The corresponding calculation process for these two contact forces is proposed here, as shown in Fig. 7.

During each compression and restitution cycle, it is important to note the following points:

1. Collision occurs when the deformation changes from  $\delta \leq 0$  to  $\delta > 0$  and the initial relative

velocity  $\dot{\delta}^-$  is greater than zero, and the initial value of the collision hysteresis damping factor  $\mu_0$  can be calculated by Eq. (23).

2. NIRV-collision occurs when the deformation changes from  $\delta \leq 0$  to  $\delta > 0$  and the initial relative velocity  $\dot{\delta}^-$  is zero, and the initial value of the collision hysteresis damping factor  $\mu_0$  can be calculated by Eq. (28) or the hysteresis damping factor from the last collision.
3. During the initialization process, both the values of  $a$  and  $b$  are set to zero, and the existing values of  $a$  and  $b$  need to be maintained during reinitialization.
4. The post- restitution coefficient  $\varepsilon_{oum}$  calculated by Eq. (15), and  $\xi_\varepsilon$  is the accuracy of  $\varepsilon_{oum}$ .
5. The formula for calculating the iteration value  $\mu_{n+1}$  of the hydrogenation damping factor can be selected based on the principle of fewer iterations.
6. In the collision restitution phase, when  $\delta \leq 0$ , or  $\delta > 0$  and  $\dot{\delta} = 0$ , the collision is end.
7. The integrations in the dynamic equations can be performed by the Runge–Kutta method of order 4 with a time step equal  $10^{-6}$  s.

### 6 Application to collision under external force

To enhance understanding of the proposed contact force calculation approach, we explore applications involving simultaneous collisions and multiple continuous collisions under external forces. Here are examples for application.

#### 6.1 Collinear collision of triple ball chain

The collinear collision system shown in Fig. 8 demonstrates simultaneous collisions. The three balls,  $B_1$ ,  $B_2$  and  $B_3$ , each have the same mass  $m = 0.5$  kg

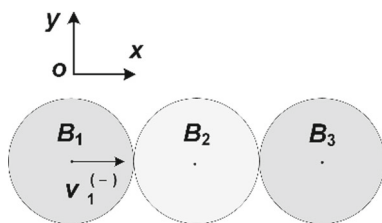


Fig. 8 Collinear collision system of triple ball chain

and radius  $R = 0.05$  m, and the contact stiffness  $k$  between  $B_1$  and  $B_2$ , as well as between  $B_2$  and  $B_3$ , is equal to  $1 \times 10^8$  N/m<sup>3/2</sup>. The ball  $B_1$  impacts  $B_2$  along the collinear direction at an initial velocity of  $x_1^{(-)} = 0.2$  m/s, while  $B_2$  and  $B_3$  are in contact before the initial collision. Using  $x_1, x_2$  and  $x_3$  to represent the displacements of  $B_1, B_2$  and  $B_3$ , with initial values of 0 m, 0.1 m and 0.2 m, respectively.

The dynamic equations of this system can be written as follows

$$\begin{cases} m\ddot{x}_1 = -F_{n1} \\ m\ddot{x}_2 = F_{n1} - F_{n2} \\ m\ddot{x}_3 = F_{n2} \end{cases} \tag{33}$$

with

$$\begin{cases} F_{n1} = k\delta_{12}^{\frac{3}{2}} + \mu_{12}\delta_{12}^{\frac{3}{2}}\dot{\delta}_{12} \\ F_{n2} = k\delta_{23}^{\frac{3}{2}} + \mu_{23}\delta_{23}^{\frac{3}{2}}\dot{\delta}_{23} \\ \delta_{12} = 2R - (x_2 - x_1) \\ \delta_{23} = 2R - (x_3 - x_2) \\ \dot{\delta}_{12} = \dot{x}_1 - \dot{x}_2 \\ \dot{\delta}_{23} = \dot{x}_2 - \dot{x}_3 \end{cases} \tag{34}$$

where  $F_{n1}$  and  $F_{n2}$  represent the contact forces between  $B_1$  and  $B_2$ , as well as between  $B_2$  and  $B_3$ , respectively, whereas  $\delta_{12}$  and  $\delta_{23}$  are the corresponding deformations,  $\dot{\delta}_{12}$  and  $\dot{\delta}_{23}$  denote the corresponding deformation velocities,  $\mu_{12}$  and  $\mu_{23}$  are the corresponding hysteresis damping factors, and the pre- restitution coefficients used to calculate the initial values of  $\mu_{12}$  and  $\mu_{23}$  are set to  $\varepsilon_{in12}$  and  $\varepsilon_{in23}$ , respectively.

The computation process in Fig. 7 is utilized to simulate the dynamic responses of the three ball, and the initial parameters of  $X_0, V_0, \varepsilon_{in12}$  and  $\varepsilon_{in23}$  are  $[0, 0.1, 0.2]^T, [0.2, 0, 0]^T, 0.8$  and  $0.7$ , respectively. The initial values of  $\mu_{12}$  and  $\mu_{23}$  are calculated by Eq. (23) with the initial velocity 0.2 m/s, with each factor requiring independent and simultaneous iteration in each cycle of calculation. After six cycles,  $\mu_{12}$  and  $\mu_{23}$  meet the required precision ( $\xi_\varepsilon = 1\%$ ). The Hunt and Crossley model, as well as Flores et al. model are also applied to simulate the same simultaneous collisions. In this simulation,  $\mu_{12}$  and  $\mu_{23}$  are equal and calculated based on the initial velocity. Then, we get the simulation results, as shown in Figs. 9, 10, 11, 12.

Figure 9 represents the velocity developments of  $B_1, B_2$  and  $B_3$ , corresponding to solid, dashed, and dotted lines, respectively. Under the collision contact



force  $F_{n1}$  shown in Fig. 10, the velocity of  $B_1$  continues to decrease from 0.2 m/s until it separates from  $B_2$ , while the velocity of  $B_3$  continues to accelerate from zero until it separates from  $B_2$  under the contact force  $F_{n2}$ . Unlike  $B_1$  and  $B_3$ ,  $B_2$  is simultaneously influenced by  $F_{n1}$  and  $F_{n2}$ . Initially,  $F_{n1}$  exceeds  $F_{n2}$ , causing  $B_2$ 's velocity to increase until it reaches its peak, then it diminishes as  $F_{n1}$  becomes less than  $F_{n2}$ , until it separates from  $B_1$  and  $B_3$ .

The velocities shown Fig. 9 are obtained based on the proposed method, and similar results can also be obtained by applying Hunt and Crossley model, and Flores et al. model. However, there are differences in the influence of different contact force models on the dynamic response of simultaneous collisions, as shown in Figs. 10, 11, 12. From Fig. 10, it can be observed that the differences in the collision contact forces  $F_{n1}$  calculated by the Hunt and Crossley model, the Flores et al. model, and the proposed method are relatively small during the compression phase, whereas the difference is relatively obvious in the restitution phase. The reasons are the different effect in  $\mu_{12}$  values and the influence of the external force  $F_{n2}$  during the restitution phase. Compared to  $F_{n1}$ , there is a significant difference in the NIRV-collision contact force  $F_{n2}$ , and the main reason is the different values of  $\mu_{23}$ . The above differences are also clearly reflected in the deformation velocity shown in Fig. 11.

Figure 12 shows the hysteresis loops of the collisions between  $B_1$  and  $B_2$ , and between  $B_2$  and  $B_3$ , respectively, denoted as the hysteresis loops  $B_{12}$  and  $B_{23}$ . This figure reveals that the  $B_{12}$  loops generated by the Flores et al. model and the proposed method are relatively similar, indicating minor differences in energy loss between these two models. Additionally,

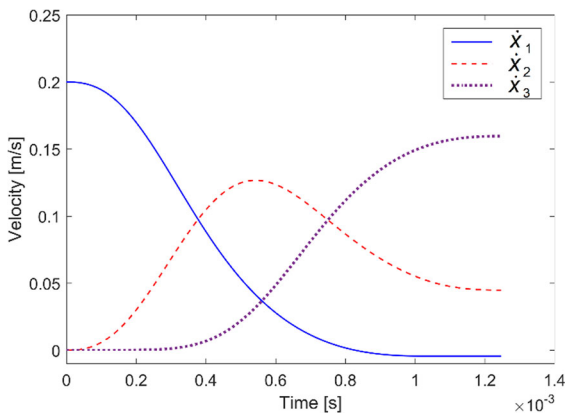


Fig. 9 Velocities of the balls

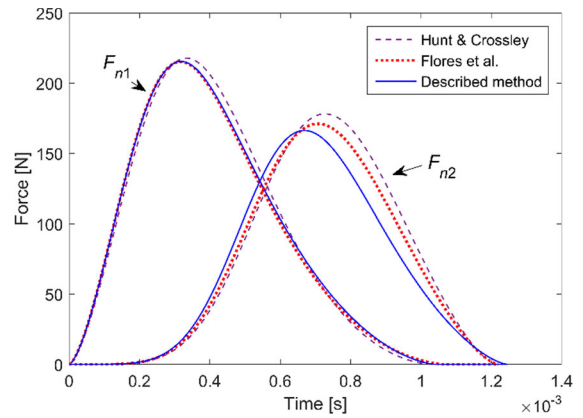


Fig. 10 Collision contact forces of the two collision

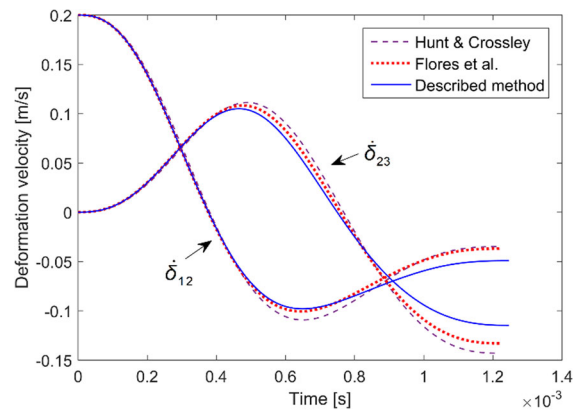


Fig. 11 Deformation velocities of the two collision

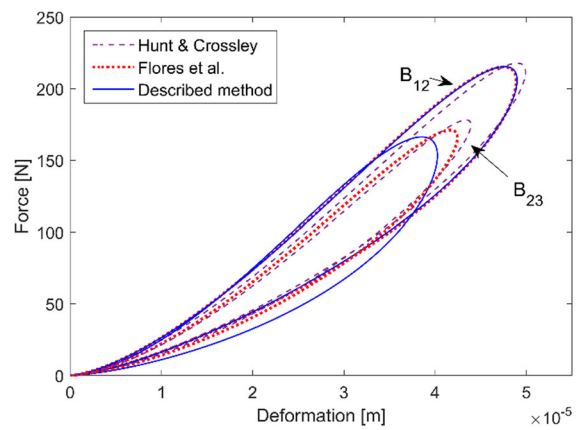


Fig. 12 Hysteresis loops of the two collisions

the post-restitution coefficients  $\epsilon_{out12}$  differ from the pre-restitution coefficients  $\epsilon_{in12}$  by less than 1%, as illustrated in Table 2. In contrast, the hysteresis loop

produced by the Hunt and Crossley model shows marked differences, with a deviation of 5.7% from the pre-restitution coefficients. For the hysteresis loops of  $B_{23}$ , the discrepancies among the Hunt and Crossley model, Flores et al. model, and the proposed method are significant, with errors in the post-and pre-restitution coefficients of 23.7%, 18.7%, and 0.8%, respectively.

It is important to note that the number of iterations required in the calculation process, as demonstrated in Fig. 7, correlates with the pre-restitution coefficient and the initial relative velocity, as shown in Table 3 which is calculated with the condition of  $\varepsilon_{in12} = \varepsilon_{in23}$ . When the values of  $\mu_{12}$  and  $\mu_{23}$  computed by Eq. (23) both meet the accuracy requirements, only one cycle calculation is required, such as  $\varepsilon_{in}$  is 0.85; otherwise, several cycles of calculation are needed. Due to the mutual influence of the two collisions, the simultaneous iteration of  $\mu_{12}$  and  $\mu_{23}$  may result in more cycles and even inability to converge marked by “-”, as shown in Table 3. In this case, it is necessary to reduce the accuracy requirements or adopt other methods.

### 6.2 Elastic ball collision under spring support and external force

When simulating multiple consecutive collisions using the computation process shown in Fig. 7, attention should be paid to initializing parameters for each collision. The system setup for this simulation involves a ball supported by a spring and external forces as depicted in Fig. 13. The ball, with a mass  $m$  of 0.5 kg, a radius  $R = 0.05$  m, and an equivalent stiffness  $k$  equal to  $1.8 \times 10^7$  N/m<sup>3/2</sup>, impacts on a rigid wall under the action of a periodic force  $F(t)$  and spring damping force. When the spring is inactive, the original coordinate system is centered at the ball, with a distance  $b$  from the ball to the wall set at 0.048 m.

**Table 2** Pre- and post- restitution coefficients

Model	$\varepsilon_{in12}$	$\varepsilon_{out12}$	$\varepsilon_{in23}$	$\varepsilon_{out23}$
Hunt and Crossley	0.8	0.8453	0.7	0.8661
Flores et al.	0.8	0.8020	0.7	0.8306
Described method	0.8	0.8067	0.7	0.7059

The following is the dynamic equivalent equation of the contact system shown in Fig. 13.

$$m\ddot{\delta} + \mu\delta^3\dot{\delta} + k\delta^3 = F(t) - (k_e x + c_e \dot{x}) \tag{35}$$

where  $x$  denotes the position of the ball and its initial value  $x_0$  is  $-0.01$  m,  $\delta$  represents the deformation between the ball and wall and it is evaluated by Eq. (36),  $k_e = 10.6$  N/m and  $c_e = 100$  N·s/m are the support spring stiffness and damping, respectively, and  $F(t)$  is the sinusoidal external force shown in Eq. (37)

$$\delta = x + R - b \tag{36}$$

$$F(t) = 500 + 250\sin(2000t) \tag{37}$$

Assuming here that the restitution coefficient of each contact process is 0.9 and setting  $\xi_e = 0.5\%$ , the simulation for each collision is initialized as per the process shown in Fig. 7. For collisions starting with initial velocity,  $V_0$  is determined at the point of collision occurs, whereas for those without initial velocity = 0 while  $X_0$  is calculated based on the timing of collision occurrence. Additionally, the iterative value of  $\mu_{n+1}$  is calculated by the Newton’s iterative formula (29), or Eq. (27) based on bisection method, and the number of iterations for the first 10 collisions is shown in the Table 4. Correspondingly, the iteration times of the method used in Sect. 6.1 are listed in the third row of this table. It can be drawn from the table that in this case, it is more optimal to apply Newton’s iterative method to calculate  $\mu_{n+1}$  before the range  $[a, b]$  is determined.

Then, we get the simulation results, as shown in Figs. 14, 15, 16, 17. Figure 14 represents the development of the ball position, including solid line acquired by the described approach, and the straight line illustrates the position of the ball at the instant of contact occurs. From this figure, it can be drawn that after several collisions, the ball adheres closely to the wall, and its distance from the center to the wall gradually decreases until it changes in a cycle since the collision consuming the elastic potential energy at the initial position. The symbols “o” and “x” which denote the start mark and the end mark of contact cycle have also evolved from separation to overlap.

Figure 15 shows the variation curves of contact force and equivalent external force, where the solid line represents the contact force and the dashed line is

**Table 3** Number of cycle calculations under different conditions

$\dot{x}_{12}^{(-)}$ (m/s)	Cycle times									
	$\epsilon_{in} = 0.95$	$\epsilon_{in} = 0.9$	$\epsilon_{in} = 0.85$	$\epsilon_{in} = 0.8$	$\epsilon_{in} = 0.75$	$\epsilon_{in} = 0.7$	$\epsilon_{in} = 0.65$	$\epsilon_{in} = 0.6$	$\epsilon_{in} = 0.55$	$\epsilon_{in} = 0.5$
0.1	8	1	1	6	7	6	5	5	3	7
0.2	6	1	1	4	7	6	5	4	-	-
0.3	27	3	1	4	6	5	6	6	5	7
0.4	8	5	1	5	6	7	5	4	5	5
0.5	16	3	1	6	6	6	5	5	4	-

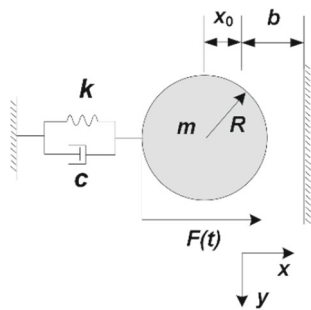


**Fig. 13** Collision system with periodic external force and spring damping force

the equivalent external force formed by the combination of spring support force and sinusoidal external force, respectively. Corresponding to Fig. 14, the contact force decreases significantly until it undergoes a constant amplitude cyclic change. It should be noted that the first 5 cycles are collision contact, and the following are NIRV-collision contact. Moreover, the equivalent external force during these collisions and NIRV-collisions also decreases, and its influence on the contact process gradually increases until basically under the influence of the equivalent external force.

**Table 4** Comparison of iteration times

$\mu_{n+1}$	Collisions										
	1th	2th	3th	4th	5th	6th	7th	8th	9th	10th	11th
Equations (27) or (29)	0	0	1	1	5	1	1	1	1	1	0
Equations (27) or (31)	0	0	7	14	22	13	18	15	10	7	4

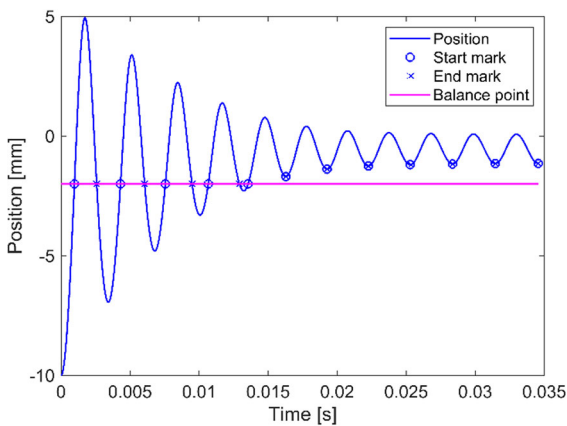


**Fig. 14** Position of the ball

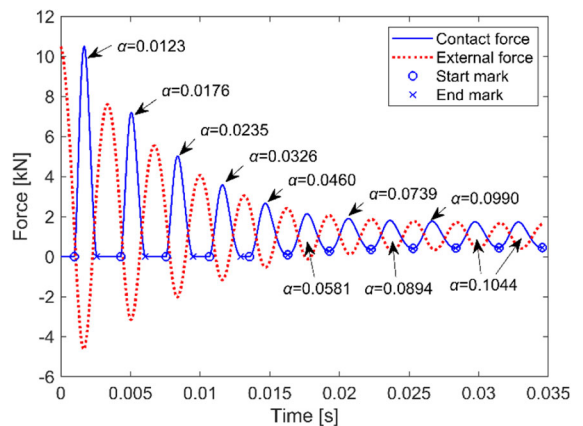


**Fig. 15** Contact force and equivalent external force

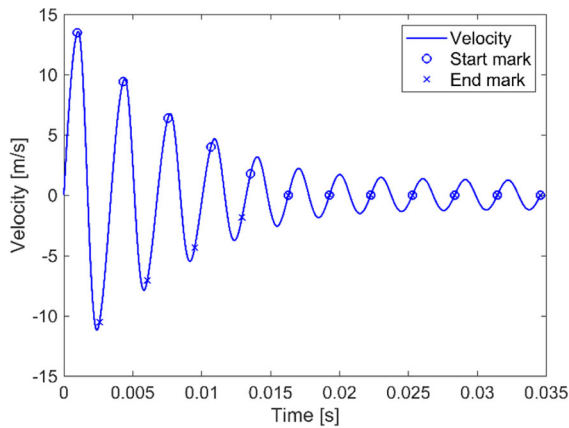


**Fig. 16** Velocity of the ball

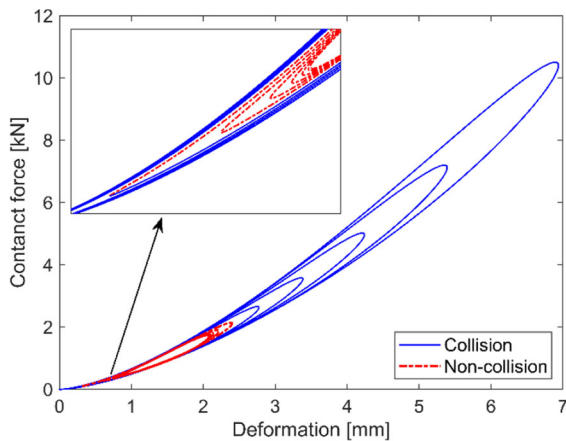


**Fig. 17** Hysteresis loop during contact process

This figure also shows that hysteresis damping factor coefficient  $\alpha$  for each contact process increases as the contact strength weakens, until to a constant value. For this constant value, the constant amplitude and variation frequency of the contact cycle are the reasons.

The plots of the ball velocity are exhibit the same trend, as shown in Fig. 16. In addition, due to the influence of the equivalent external force, the difference between the initial approach velocity and the maximum approach velocity during contact process is increased as the initial approach velocity decreases. When the initial approach velocity is equal to zero, the approach velocity changes with the variation of the equivalent external force.

It can be observed from Figs. 14, 15, 16, 17 that the area of hysteresis loop is decreased with the reduction of the distance between the ball and the wall. The

sources of the energy loss represented by the hysteresis loop of the first 5 collision contact are the initial relative kinetic energy and the work done by the equivalent external force, whereas other contact processes are only come from the work done by the equivalent external force. It should be highlight that the first four collision hysteresis loops are closed curves that change from the origin to the origin, and the fifth collision hysteresis loop changes from the origin to a non-origin, whereas the subsequent hysteresis loops change from a non-origin to a non-origin.

## 7 Conclusion

For unstable mechanical systems, the calculation for collision and NIRV-collision contact forces between elastic spheres was studied. Initially, brief issues of the continuous contact force models associated with the fundamental contact mechanics and energy conversion during contact process were illustrated. Next, the collision process without external forces was studied, and a corresponding hysteresis damping factor model was established combining with energy restitution coefficient and numerical computation. On these bases, the bisection method, Newton's method and energy restitution coefficient were applied to construct an iterative formula for the hysteresis damping factor, and then a collision and NIRV-collision contact force calculation approach was established, whereas corresponding numerical calculation process was also proposed. Finally, the proposed approach was applied to simulate the collision and NIRV-collision contact dynamics of simultaneous collisions and multiple continuous collisions, and the characteristics of the elastic balls in these systems were analyzed, including displacement, contact force, equivalent external force, velocity, and hysteresis loop. The results indicate:

- (1) The proposed collision hysteresis damping factor without external forces can achieve high accuracy even with low recovery coefficients.
- (2) The calculation approach established in this article can be well applied to collision and NIRV-collision dynamic analysis.
- (3) The energy loss law of periodic NIRV-collision contact can be described by the Strong's energy model.

**Acknowledgements** This work was supported by the National Natural Science Foundation of China (51975323).

**Author contributions** All authors contributed to the study conception and design. Material preparation, data collection and analysis were performed by Yinhua Shen and Dong Xiang. The first draft of the manuscript was written by Yinhua Shen and all authors commented on previous versions of the manuscript. All authors read and approved the final manuscript.

**Funding** The authors have not disclosed any funding.

**Data availability** No datasets were generated or analysed during the current study.

#### Declarations

**Conflict of interest** The authors declare no competing interests.

#### References

- Gilardi, G., Sharf, I.: Literature survey of contact dynamics modelling. *Mech. Mach. Theory* **37**(10), 1213–1239 (2002). [https://doi.org/10.1016/s0094-114x\(02\)00045-9](https://doi.org/10.1016/s0094-114x(02)00045-9)
- MacHado, M., Moreira, P., Flores, P., Lankarani, H.M.: Compliant contact force models in multibody dynamics: evolution of the Hertz contact theory. *Mech. Mach. Theory* **53**, 99–121 (2012). <https://doi.org/10.1016/j.mechmachtheory.2012.02.010>
- Skrinjar, L., Slavič, J., Boltežar, M.: A review of continuous contact-force models in multibody dynamics. *Int. J. Mech. Sci.* **145**, 171–187 (2018). <https://doi.org/10.1016/j.ijmecsci.2018.07.010>
- Corral, E., Moreno, R.G., García, M.J.G., et al.: Nonlinear phenomena of contact in multibody systems dynamics: a review. *Nonlinear Dyn.* **104**(2), 1269–1295 (2021). <https://doi.org/10.1007/s11071-021-06344-z>
- Wu, D., Han, Q., Wang, H., et al.: Nonlinear dynamic analysis of rotor-bearing-pedestal systems with multiple fit clearances. *IEEE Access* **8**, 26715–26725 (2020). <https://doi.org/10.1109/ACCESS.2020.2971326>
- Flores, P., Ambrósio, J.: On the contact detection for contact-impact analysis in multibody systems. *Multibody Syst. Dyn.* **24**, 103–122 (2010). <https://doi.org/10.1007/s11044-010-9209-8>
- Khulief, Y.A., Shabana, A.A.: A continuous force model for the impact analysis of flexible multibody systems. *Mech. Mach. Theory* **22**, 213–224 (1987). [https://doi.org/10.1016/0094-114X\(87\)90004-8](https://doi.org/10.1016/0094-114X(87)90004-8)
- Hunt, K.H., Crossley, F.R.E.: Coefficient of restitution interpreted as damping in vibroimpact. *J. Appl. Mech.* **42**(2), 440–445 (1975). <https://doi.org/10.1115/1.3423596>
- Lee, T.W., Wang, A.C.: On the dynamics of intermittent-motion mechanisms. Part I: dynamic model and response. *ASME. J. Mech. Trans. Autom.* **105**, 534–540 (1983). <https://doi.org/10.1115/1.3267392>
- Lankarani, H.M., Nikraves, P.E.: A contact force model with hysteresis damping for impact analysis of multibody systems. *J. Mech. Des.* **112**(3), 369–376 (1990). <https://doi.org/10.1115/1.2912617>
- Gonthier, Y., McPhee, J., Lange, C., et al.: A regularized contact model with asymmetric damping and dwell-time dependent friction. *Multibody Syst. Dyn.* **11**, 209–233 (2004)
- Gharib, M., Hurmuzlu, Y.: A new contact force model for low coefficient of restitution impact. *J. Appl. Mech.* **79**, 064506 (2012). <https://doi.org/10.1115/1.4006494>
- Safaeifar, H., Farshidianfar, A.: A new model of the contact force for the collision between two solid bodies. *Multibody Syst. Dyn.* **50**, 233–257 (2020). <https://doi.org/10.1007/s11044-020-09732-2>
- Zhao, P., Liu, J., Li, Y., et al.: A spring-damping contact force model considering normal friction for impact analysis. *Nonlinear Dyn.* **105**(6), 1437–1457 (2021). <https://doi.org/10.1007/s11071-021-06660-4>
- Zhang, J., Liang, X., Zhang, Z., et al.: A continuous contact force model for impact analysis. *Mech. Syst. Signal Pr.* **168**, 108739 (2022). <https://doi.org/10.1016/j.ymsp.2021.108739>
- Kildashti, K., Dong, K., Yu, A.: Contact force models for non-spherical particles with different surface properties: a review. *Powder Technol.* **418**, 118323 (2023). <https://doi.org/10.1016/j.powtec.2023.118323>
- Zhang, Y., Ding, Y., Xu, G.: A continuous contact-force model for the impact analysis of viscoelastic materials with elastic aftereffect. *Multibody Syst. Dyn.* **61**, 435–451 (2024). <https://doi.org/10.1007/s11044-023-09954-0>
- Shen, Y., Xiang, D., Wang, X., et al.: A contact force model considering constant external forces for impact analysis in multibody dynamics. *Multibody Syst. Dyn.* **44**(4), 397–419 (2018). <https://doi.org/10.1007/s11044-018-09638-0>
- Stronge, W.J.: Rigid body collisions with friction. *Proc. Royal Soc. Lond., Series A Math. Phys. Sci.* **431**, 169–181 (1990)
- Ajmi, M., Velez, P.: A model for simulating the quasi-static and dynamic behavior of solid wide-faced spur and helical gears. *Mech. Mach. Theory* **40**(2), 173–190 (2009). <https://doi.org/10.1016/j.mechmachtheory.2003.06.001>
- Chen, S., Tang, J., Wu, L.: Dynamics analysis of a crowned gear transmission system with impact damping: based on experimental transmission error. *Mech. Mach. Theory* **74**(6), 354–369 (2014). <https://doi.org/10.1016/j.mechmachtheory.2014.01.003>
- Yu, X., Sun, Y., Li, H., et al.: An improved meshing stiffness calculation algorithm for gear pair involving fractal contact stiffness based on dynamic contact force. *Eur. J. Mech. A. Solids* **94**, 104595 (2022). <https://doi.org/10.1016/j.euromechsol.2022.104595>
- Warzecha, M.: An investigation of compliant contact force models applied for simultaneous, multi-zone impacts of particles. *Comp. Part. Mech.* **11**, 1–27 (2024). <https://doi.org/10.1007/s40571-023-00606-w>
- Michalczyk, J.: Phenomenon of force impulse restitution in collision modelling. *J. Theor. Appl. Mech.* **46**(4), 897–908 (2008)
- Carretero-González, R., Khatri, D., Porter, M.A., Kevrekidis, P.G., Daraio, C.: Dissipative solitary waves in granular

- crystals. *Phys. Rev. Lett.* **102**(2), 024102 (2009). <https://doi.org/10.1103/PhysRevLett.102.024102>
26. Flores, P., Machado, M., Silva, M.T., et al.: On the continuous contact force models for soft materials in multibody dynamics. *Multibody Syst. Dyn.* **25**(3), 357–375 (2011). <https://doi.org/10.1007/s11044-010-9237-4>
27. Hu, S., Guo, X.: A dissipative contact force model for impact analysis in multibody dynamics. *Multibody Syst. Dyn.* **35**(2), 131–151 (2015). <https://doi.org/10.1007/s11044-015-9453-z>

**Publisher's Note** Springer Nature remains neutral with regard to jurisdictional claims in published maps and institutional affiliations.

Springer Nature or its licensor (e.g. a society or other partner) holds exclusive rights to this article under a publishing agreement with the author(s) or other rightsholder(s); author self-archiving of the accepted manuscript version of this article is solely governed by the terms of such publishing agreement and applicable law.